RSC Advances

PAPER

View Article Online
View Journal | View Issue

Cite this: *RSC Adv.*, 2025, **15**, 32821

Design, synthesis and molecular modeling of new coumarin–thiazole derivatives as dual EGFR/HDAC1 inhibitors: *in vitro* and *in vivo* anticancer assays

Eman Y. Ahmed, *[a] Mai M. Elghonemy,[a] Rasha Z. Batran, *[a] Manar E. A. Elasasy,[b] Sherien M. El-Daly, [cd] Marwa A. Mahmoud,[c] Hanem M. Awad [de] and Nehad A. Abdel Latif*[a]

Received 20th June 2025
Accepted 25th August 2025

DOI: 10.1039/d5ra04395f

rsc.li/rsc-advances

The growing evidence ascertaining the overexpression of EGFR and HDAC1 in breast and colorectal cancers prompted us to design and synthesize some new coumarin–thiazole derivatives with dual EGFR/HDAC1 inhibitory activity, considering the nature of EGFR and HDAC inhibitory models. The new derivatives were evaluated for their *in vitro* cytotoxicity against HCT-116 and MCF-7 cancer cells along with BJ-1 normal cells. Compound 3-(-1-((-5-(-(4-bromophenyl)diazenyl)-4-methylthiazol-2(3*H*)-ylidene) hydrazono)ethyl)-4-hydroxy-2*H*-chromen-2-one (**3m**) showed promising selectivity indices for both cell lines, preferential inhibition of EGFR/HDAC1/ERK, induction of cell cycle arrest and apoptosis, and significant *in vivo* antitumor activity against Ehrlich ascites and solid carcinoma models. Docking study showed that the selected compound attained promising results within the active sites of EGFR and HDAC1.

1. Introduction

The pathophysiology of tumors is extremely complicated, and malignancies, in general, exhibit relapse and resistance traits.[1,2] While numerous therapeutic targets have been identified, single-target medications generally provide transient and inadequate clinical efficacy.[3–5] In contrast, multi-target medications have the potential to address the issues of cancer resistance and recurrence by concurrently focusing on several biological molecules and signal pathways implicated in tumor development, thereby enhancing the anticancer activity through additive or synergistic mechanisms.

The first growth-factor receptor tyrosine kinase to be discovered in cancer is the epidermal growth factor receptor (EGFR), which controls a number of intracellular functions such as cell survival, differentiation, and proliferation. Breast, colon, prostate, and non-small cell lung cancers are among the tumors that can be treated by targeting the EGFR.[6] On the other hand, histone deacetylases (HDACs), as epigenetic targets for the design of cancer therapeutics, are divided into four classes: class I consists of HDAC-1, -2, -3, and -8; class II includes HDAC-4, -5, -7, -6, -9, and -10; class IV contains HDAC-11 only; and class III HDACs, named sirtuins, consist of seven different members (SIRT-1–7).[7] These enzymes are generally responsible for deacetylating lysine residues of histone and nonhistone proteins, which control gene expression. Oncogenic HDAC-containing transcriptional complexes and the aberrant expression or activity of HDACs have been implicated in a variety of cancers, with HDAC1 being specifically upregulated in breast, colon, liver and lung cancers.[8,9]

It is noteworthy that HDAC inhibitors have been shown to reduce EGFR expression in colorectal cancer cells; furthermore, EGFR inhibitor resistance may be overcome with the use of HDAC inhibitors. Compared with single inhibitors, the combination of erlotinib and HDAC inhibitors has demonstrated significant reductions in tumor growth and tumor weight in EGFR-resistant NSCLC cells.[10,11] An examination of the pharmacophoric features of EGFR and HDAC inhibitors showed that they share three main features: (i) a heterocyclic aromatic cap that can form hydrogen bonds with the essential amino acids and occupy the EGFR adenine binding pocket and the narrow tubular pocket of HDAC, (ii) an amide linker that can occupy the linker region of both proteins and (iii) a terminal hydrophobic group that can be inserted in the hydrophobic region of EGFR

[a]*Chemistry of Natural Compounds Department, Pharmaceutical and Drug Industries Research Institute, National Research Centre, Dokki, Cairo, 12622, Egypt. E-mail: eyam_ha@yahoo.com; rasha_batran@yahoo.com; nehad_km@yahoo.com*

[b]*Applied Organic Chemistry Department, National Research Centre, Dokki, Cairo, 12622, Egypt*

[c]*Medical Biochemistry Department, Medical Research and Clinical Studies Institute, National Research Centre, Cairo, Egypt*

[d]*Cancer Biology and Genetics Laboratory, Centre of Excellence for Advanced Sciences, National Research Centre, Cairo, Egypt*

[e]*Tanning Materials and Leather Technology Department, National Research Centre, Dokki, Cairo, 12622, Egypt*

and help in the stabilization of the compound in the HDAC pocket (Fig. 1).[12–14]

Coumarins have a broad range of pharmacological activities due to their capacity to induce non-covalent interactions, including hydrogen bonds, metal coordination, Van der Waals force, and electrostatic interactions, with numerous proteins. The reactivity of pyrone and benzene rings and the simple chemical structure of coumarins are particularly appealing because the electrical environments of these types of bioactive molecules are controlled by the presence of conjugated double bonds.[15] By blocking several cancer-related receptors and enzymes, such as EGFR and HDAC1, coumarins and their bioisosteres (*e.g.* erlotinib, **I**, tasquinimod and **II**) can efficiently exert their pronounced antitumor effects (Fig. 1).[16–18]

Furthermore, nitrogen-containing heterocyclic compounds, which make up more than 60% of novel drugs and are essential to anticancer research because of their flexible and dynamic cores, have been the focus of medicinal chemists for so long. Thiazole derivatives, as the most common and important heterocyclic molecules in most marketed pharmaceuticals, with a high degree of structural diversity, exhibit a variety of mechanisms for inhibiting cancer, such as targeting the EGFR (*e.g.* dasatinib and dabrafenib)[6] and HDAC (*e.g.* **III** and **IV**) proteins (Fig. 1).[19,20]

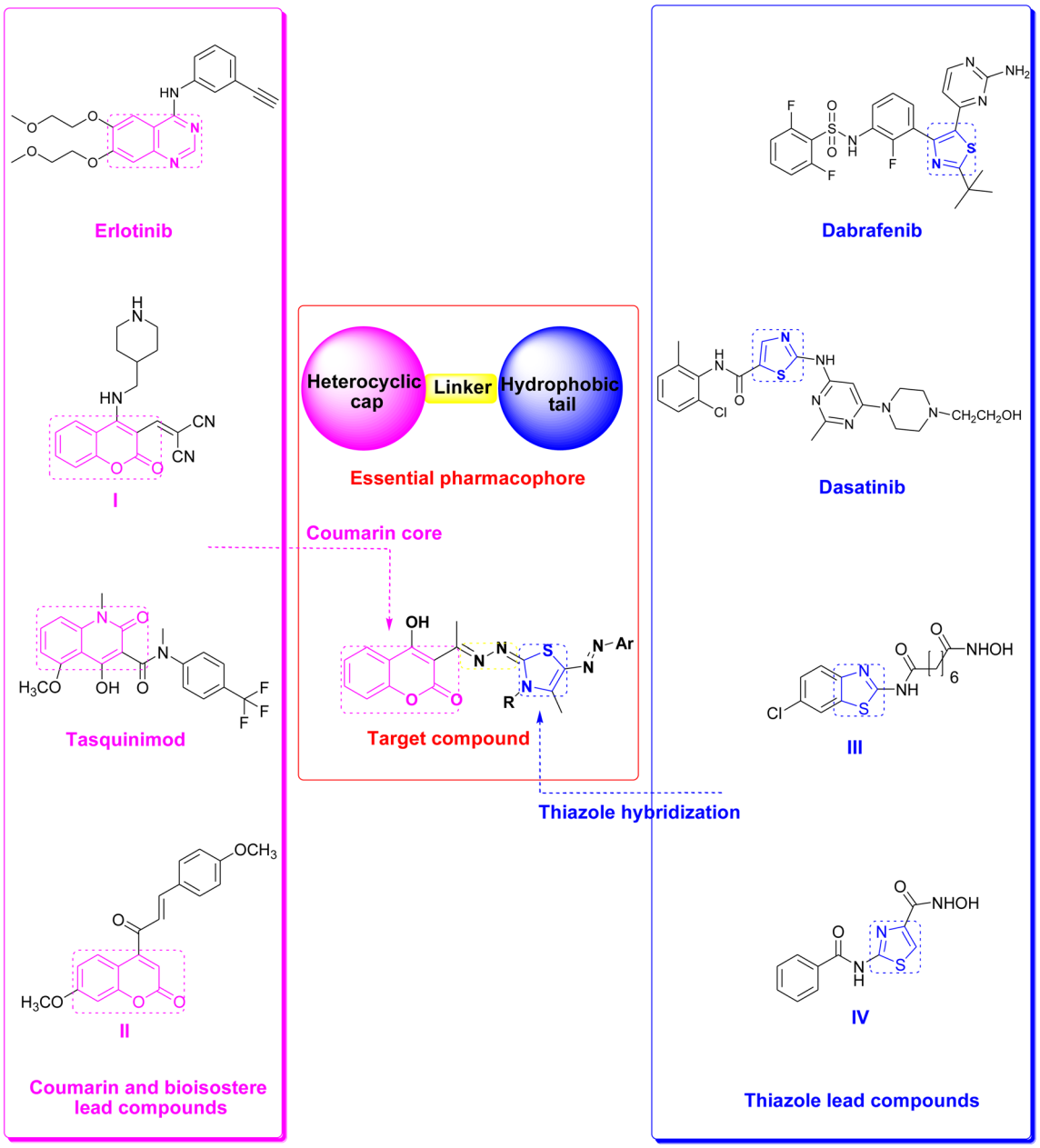

Fig. 1 Reported EGFR and HDAC inhibitors and the design of the newly synthesized coumarin derivatives.

Coumarin–thiazole hybrids are advantageous as dual EGFR/HDAC1 inhibitors when compared with reported inhibitors, such as hydroxamic acids, trimethoxyphenyl chalcones, aminoquinolines and quinazolines. Hydroxamic acids, though known for their pronounced zinc-chelating ability, are associated with poor oral bioavailability, metabolic instability and toxicity, while trimethoxyphenyl chalcones exhibit non-specific binding and limited selectivity.[21,22] In comparison, incorporating coumarin and thiazole within a single molecular framework facilitates the development of dual inhibitors with improved efficacy, enhanced pharmacokinetic characteristics, increased selectivity, and less toxicity.[23–25] On the other hand, quinazolines may be associated with resistance mechanisms, including mutations at the EGFR kinase domain, which can restrict their long-term effectiveness, while coumarin-based scaffolds can bypass such resistance mechanisms and demonstrate broader efficacy in resistant cancer cell lines.[26,27] Unlike aminoquinolines, which frequently need extra modifications to interact with HDAC or EGFR, the coumarin–thiazole scaffold simply accommodates dual binding through a strategic orientation of donor–acceptor groups, ensuring better structural diversity for optimization.[23]

In continuation to our previous studies concerning biologically active natural compounds,[28–30] a new series of coumarin-based thiazole derivatives was designed and synthesized featuring the main pharmacophores of the clinically used and reported EGFR and HDAC inhibitors. The designed compounds comprised three moieties: (i) a coumarin ring as the heterocyclic aromatic cap, (ii) a linker region where the amide linker of the lead compounds was modified to be methylenehydrazine, and (iii) a terminal hydrophobic group consisting of different aromatic moieties. The purpose of this study was to observe the effects of different substituents on the anticancer activity of potential dual inhibitors and to emphasize the activity of the promising compounds.

2. Results and discussion

2.1. Chemistry

The target 3-(-1-((5-(aryl)diazenyl)thiazol-2(3*H*)-ylidene)-hydrazono)ethyl)-4-hydroxy-coumarin derivatives **3a–o** were synthesized *via* the cyclo-condensation of the thiosemicarbazone intermediates **2a–c** with different aryl-hydrazonoyl chlorides in an alkaline medium, as outlined in Scheme 1. The

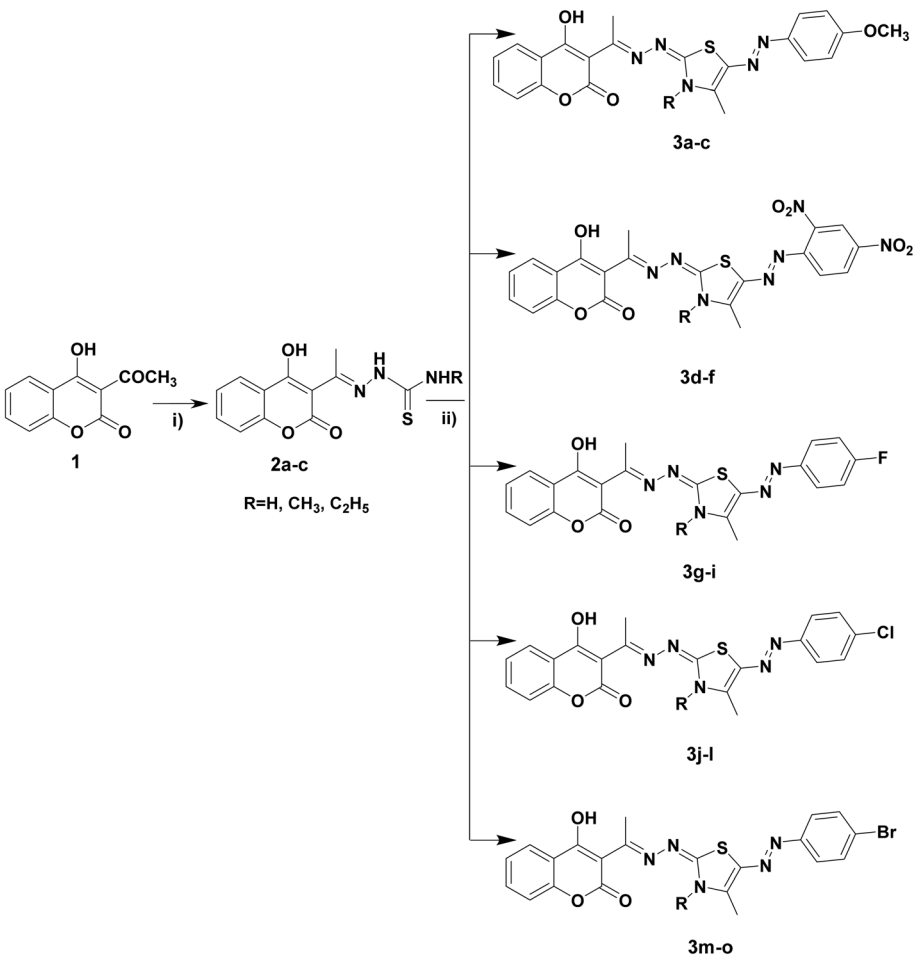

Scheme 1 (i) $NH_2NHCSNHR$, EtOH, AcOH, reflux and (ii) $CH_3COCH(Cl)N{=}N{-}Ar$, dioxane, $N(C_2H_5)_3$.

chemical structures of the newly synthesized target compounds were assigned using elemental and spectral analyses (Materials and methods section).

2.2. Biology

2.2.1 *In vitro* studies

2.2.1.1. Antiproliferative activity. Fifteen new compounds were examined for their activity against breast (MCF-7) and colorectal (HCT-116) human cancer cells and non-tumor fibroblast-derived cells (BJ-1) using the LDH assay with specific modifications, as described in the materials and methods section. In case of the MCF-7 and HCT-116 carcinoma cells, the new compounds showed remarkable IC_{50} values ranging from 2.6 to 33.8 μM. Regarding BJ-1, three compounds, in the order of **3m**, **3n** and **3o**, showed non-significant toxic activities on the healthy cells and very promising selectivity indices (Table 1).

Table 1 Antiproliferative IC_{50} values of the new compounds on the human cell lines according to the LDH assay

	IC_{50} (μM) ± SD		
Compound code	MCF-7	HCT-116	BJ-1
3a	3.1 ± 0.1	3.2 ± 0.1	24.8 ± 2.1
3b	5.0 ± 0.2	2.6 ± 0.1	27.0 ± 2.2
3c	2.6 ± 0.1	3.1 ± 0.1	27.0 ± 2.1
3d	5.1 ± 0.2	2.8 ± 0.1	26.7 ± 2.3
3e	3.0 ± 0.1	2.7 ± 0.1	27.1 ± 2.3
3f	2.6 ± 0.1	2.9 ± 0.2	25.6 ± 2.5
3g	2.9 ± 0.2	2.8 ± 0.2	30.6 ± 3.3
3h	2.8 ± 0.2	3.0 ± 0.2	27.5 ± 2.5
3i	3.0 ± 0.1	3.1 ± 0.2	34.3 ± 2.5
3j	3.1 ± 0.2	12.7 ± 1.2	27.0 ± 2.3
3k	5.4 ± 0.3	11.6 ± 1.1	25.8 ± 2.1
3l	4.8 ± 0.3	2.8 ± 0.1	26.2 ± 2.4
3m	12.7 ± 1.1	33.8 ± 3.1	>500
3n	12.3 ± 1.2	31.8 ± 3.3	>500
3o	22.9 ± 2.3	29.8 ± 2.5	>500
Doxorubicin	5.6 ± 0.3	6.5 ± 0.5	32.1 ± 3.1

2.2.1.2. EGFR and HDAC1 inhibition assays. EGFR and HDAC1 inhibition assays were performed for the promising compounds **3m** and **3n**. Compound **3m** revealed EGFR inhibitory activity with an IC_{50} value of 0.08 ± 0.003 μM and HDAC1 inhibition with an IC_{50} value of 1.013 ± 0.034 μM compared with the values for the reference inhibitors erlotinib (IC_{50} = 0.052 ± 0.002 μM) and TSA (IC_{50} = 0.320 ± 0.011 μM), respectively. On the other hand, compound **3n** demonstrated EGFR and HDAC1 enzymatic inhibition with IC_{50} values of 0.35 ± 0.011 μM and 3.879 ± 0.131 μM, respectively, showing that compound **3m** offered a better inhibitory activity in both assays.

2.2.1.3. ERK activity assay. Compound **3m**, which exhibited significant inhibitions against EGFR and HDAC1, was selected for further screening on ERK. HDAC inhibitors downregulate EGFR expression and attenuate ERK signaling, potentially disrupting the downstream signaling pathway. The results of the ERK inhibition assay revealed a considerable inhibitory activity of compound **3m** (IC_{50} = 0.339 ± 0.013 μM) relative to pluripotin (reference compound), which showed an IC_{50} value of 0.171 ± 0.006 μM.

2.2.1.4. Cell-cycle inhibition. To investigate the impact of compound **3m** on cell-cycle dynamics, MCF-7 cells were treated with it and subsequently analyzed *via* flow cytometry using propidium iodide (PI) staining. The distribution of cells across different phases of the cell cycle was quantified and compared with that of the control cells. Results revealed that the investigated compound **3m** inhibited the proliferation of MCF-7 cells by inducing a 29.71% cell-growth arrest at the G2/M phase (Fig. 2ii) compared with the 10.98% observed in the control cells (Fig. 2i). This change indicates that compound **3m** induces cell-cycle arrest by potentially disrupting the mitotic progression.

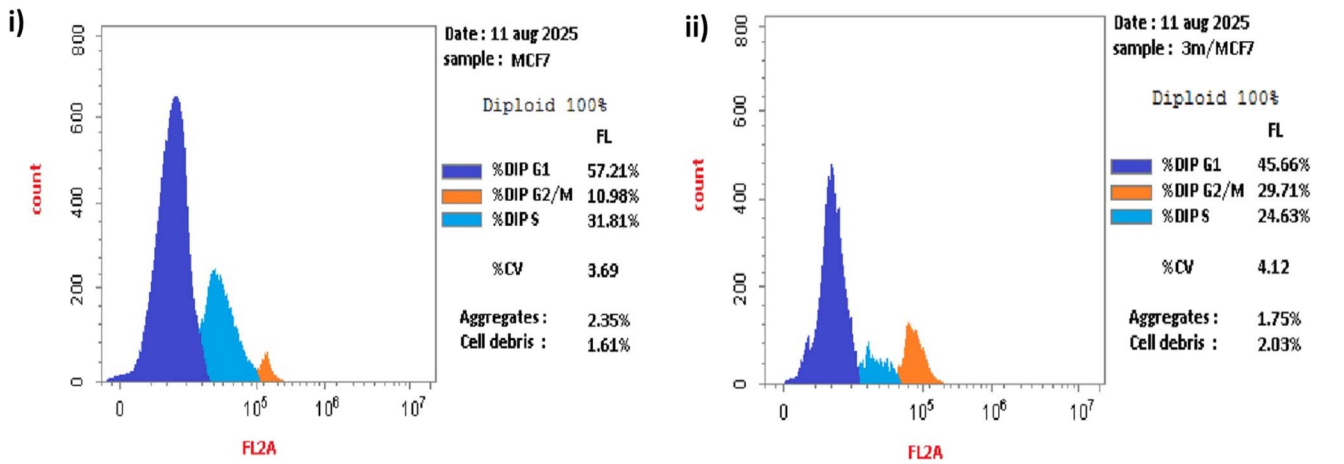

Fig. 2 Effect of compound **3m** on cell-cycle dynamics in MCF-7 cells. Flow cytometry histograms showing the DNA content profiles of the MCF-7 cells stained with propidium iodide (PI). (i) Untreated control cells exhibiting a typical distribution with the majority of the cells in the G1 phase (57.21%), followed by the S phase (31.81%) and the G2/M phase (10.98%). (ii) Cells treated with compound **3m** showing a marked accumulation of cells in the G2/M phase (29.71%) and a reduction in both the G1-phase (45.66%) and S-phase (24.63%) populations, indicating G2/M-phase arrest. Data represent one representative experiment with diploid populations and minimal debris or aggregates.

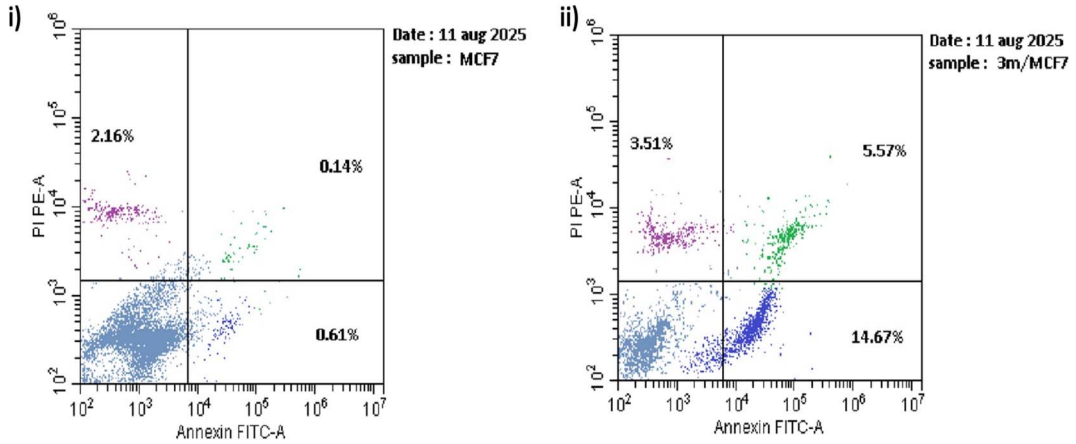

Fig. 3 Flow cytometric analysis of apoptosis in MCF-7 cells using Annexin V-FITC/PI dual staining. Cells were either left untreated (i) or treated with **3m** (ii) for the indicated treatment period (48 h). Control MCF-7 cells displayed minimal apoptosis (0.61% in early and 0.14% in late apoptosis), whereas cells treated with **3m** showed a marked increase in apoptosis (14.67% in early and 5.57% in late apoptosis), indicating apoptosis as the predominant mode of cell death.

Table 2 Effect of the administration of **3m** and **3n** on Ehrlich ascites carcinoma[a]

Groups	% change in body weight	Avg. volume of ascitic fluid (mL) [packed cell volume]	Viable cell count ($\times 10^6$ cells per mL)	Cell-growth inhibition (%)
EAC control	25.50%	10.5	33	
EAC + DOX	5%	4	9	72.72%
EAC + **3m**	8.50%	6	13	60.61%
EAC + **3n**	19.40%	8	22	33.33%

[a] The percentage change in body weight is calculated as the difference between the initial and final body weights of the same mouse.

The reduction in the S-phase cell population may suggest impaired DNA synthesis or a block prior to S-phase entry.

2.2.1.5. Cell apoptosis. Apoptosis induction in MCF-7 cells following treatment with compound **3m** was evaluated by Annexin V-FITC/PI flow cytometry. In the control cells, the majority of the population remained viable, with only 0.61% in early apoptosis, 0.14% in late apoptosis, and 2.16% in necrosis (Fig. 3i). In contrast, the MCF-7 cells treated with compound **3m** exhibited a marked increase in apoptotic fractions, with 14.67% in early apoptosis, 5.57% in late apoptosis, and 3.51% in necrosis (Fig. 3ii). These findings indicate that our synthetic drug **3m** predominantly triggers apoptotic rather than necrotic cell death, with a substantial effect on early apoptosis induction.

2.2.2 *In vivo* studies

2.2.2.1. Ehrlich ascites carcinoma model. The *in vivo* anti-tumor activities of compounds **3m** and **3n** were evaluated in female BALB/c mice following inoculation with 1×10^6 viable Ehrlich ascites carcinoma (EAC) cells. The mice were randomized into the following groups ($n = 8$ per group) and treated as follows:

- EAC Control (EAC): EAC-bearing mice treated with vehicle (DMSO).
- EAC + doxorubicin (EAC + DOX): EAC-bearing mice treated with doxorubicin i.p. injection (2 mg kg^{-1} bwt once weekly $\times$ 2 weeks).
- EAC + compound **3m** (EAC + **3m**): EAC-bearing mice treated with compound **3m**, intraperitoneal injection (2 mg kg^{-1} bwt twice weekly $\times$ 2 weeks).
- EAC + compound **3n** (EAC + **3n**): EAC-bearing mice treated with compound **3n**, intraperitoneal injection (2 mg kg^{-1} bwt twice weekly $\times$ 2 weeks).

At the end of the study, the ascitic fluid was collected and the total volume was measured. Results revealed that treatment with compounds **3m** and **3n** resulted in a significant reduction

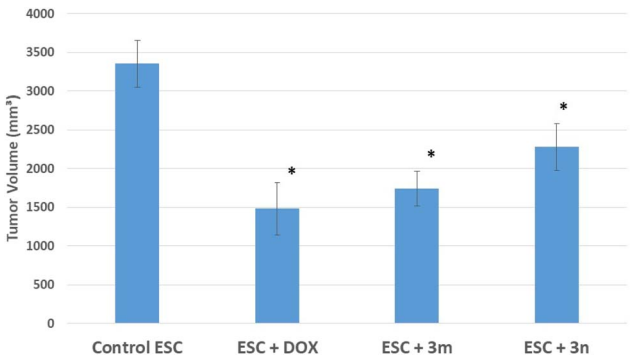

Fig. 4 Effect of the administration of compounds **3m** and **3n** on the tumor volume of Ehrlich solid carcinoma. * Significance is set at $p < 0.05$ compared to control ESC.

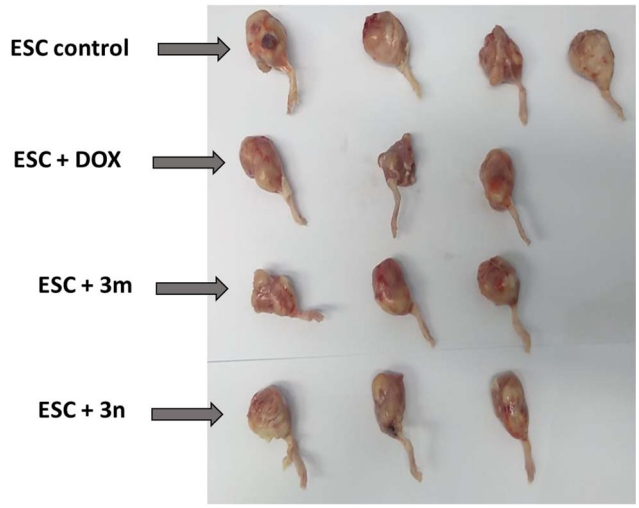

Fig. 5 Representative image showing the effect of administration of **3m** and **3n** on the volume of tumor-induced Ehrlich solid carcinoma (ESC). [Images were taken before tumor excision].

Table 3 Docking results of the co-crystalized ligands

Target protein	Co-crystallized ligand	Docking score (S) in kcal mol^{-1}	RMSD in Å
EGFR	Erlotinib	−6.6	1.851
Histone deacetylase	SAHA	−9.3	1.9

in the total volume of collected ascitic fluid. Moreover, a significant inhibition in cell growth was recorded for mice treated with compounds **3m** and **3n** by 60.61% and 33.33%, respectively, compared with mice treated with doxorubicin, which showed a 72.72% cell growth inhibition (Table 2). It could be concluded that compound **3m** was more effective in inhibiting tumor growth than compound **3n**.

2.2.2.2. Ehrlich solid carcinoma model. To assess the antitumor effects of compounds **3m** and **3n** on solid tumors *in vivo*, the Ehrlich solid carcinoma (ESC) model was used. Male BALB-c mice were inoculated intramuscularly with 2×10^6 viable Ehrlich ascites carcinoma cells to induce Ehrlich solid carcinoma. Treatment was started five days after EAC inoculation to allow for tumor establishment. All treatments were administered intratumorally. Mice were divided into the following groups:

- Normal group: mice received no EAC cells and no treatment.
- ESC control (vehicle): tumor-bearing mice treated with DMSO.
- ESC + doxorubicin: tumor-bearing mice treated with doxorubicin at a dose of 2 mg kg^{-1} once weekly for two weeks.
- ESC + compound **3m** (ESC + **3m**): tumor-bearing mice treated with compound **3m** (2 mg kg^{-1}), two doses weekly for two weeks.
- ESC + compound **3n** (ESC + 3n): tumor-bearing mice treated with compound **3n** (2 mg kg^{-1}), two doses weekly for two weeks.

Following the treatment period, the reduction in tumor volume was more significant in the group administered with compound **3m** than in the group administered with compound **3n**. Notably, the tumor size in the group treated with compound **3m** was reduced to a level comparable to that of the doxorubicin group. It could be concluded that compound **3m** was more effective in inhibiting solid tumor growth than compound **3n** (Fig. 4 and 5).

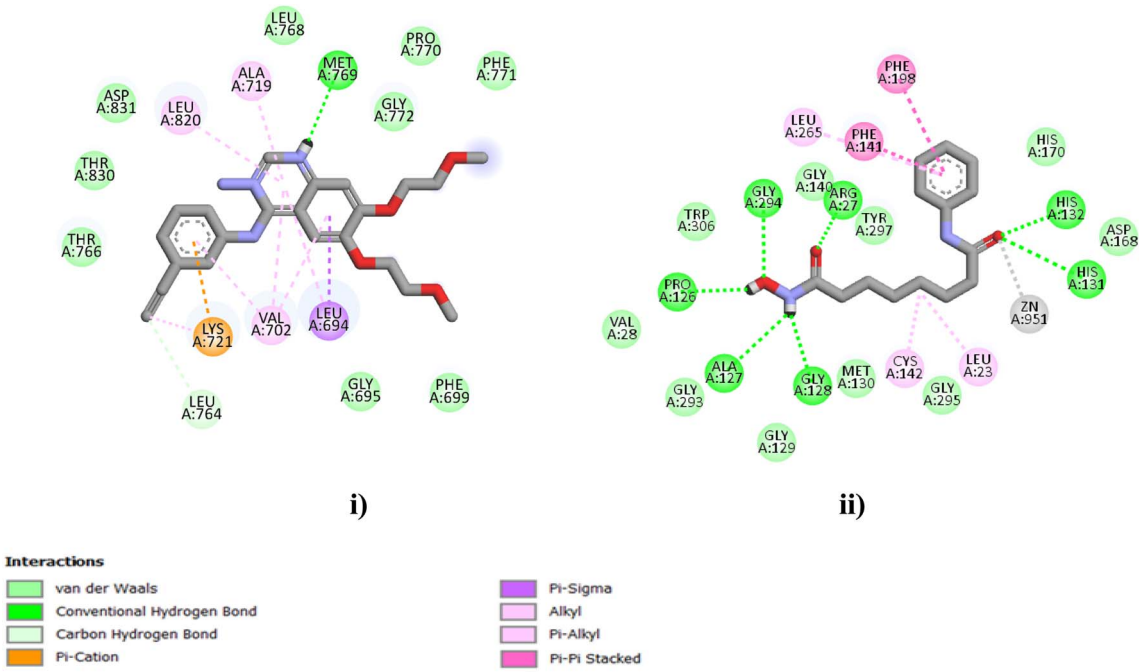

Fig. 6 (i) 2D interactions of erlotinib within the EGFR active site and (ii) SAHA within the HDAC active site.

2.3. Molecular docking

In order to examine the possible ligand-structure/enzyme-binding relationships, the promising compound **3m** was docked into the active sites of EGFR and HDAC. Molecular docking of the selected compound was accomplished using Autodock Vina. The docking setup was first validated by self-docking of the co-crystallized ligand in the vicinity of the binding site of the target enzyme, and the docking scores (S) and root mean square deviation (RMSD) are recorded in Table 3, Fig. 6i and 6ii.

The docking study showed that the tested compound attained promising results. Compound **3m** was enclosed within the active site of EGFR, with a docking score of −8.2 kcal mol^{-1}. The carbonyl moiety of the coumarin scaffold formed a hydrogen bond with Met769. The amino acid Asp831 revealed a π-anion interaction with the N=N and thiazole moieties. Moreover, the coumarin scaffold illustrated a π–σ interaction with Leu694. On the other hand, the binding of compound **3m** within the active site of HDAC ($S = -9.0$ kcal mol^{-1}) showed that the compound formed hydrogen bonds with His132, Gly295, Gly129 and Tyr297, while the coumarin scaffold interacted with Arg27, Leu23 and Cys142. The results are summarized in Table 4. The 2D representations of the docked poses along with those of the co-crystallized ligands are illustrated in Fig. 7 and 8.

Table 4 Docking results of compound **3m**

Compound	Protein	S (kcal mol^{-1})	Amino acids involved	Interacting groups/fragments	Type of interaction
3m	EGFR	−8.2	Met769	C=O	H-bond
			Asp831	N=N	π-anion
			Asp831	Thiazole	π-anion
			Phe699	Phenyl	π–π stack
			Leu694	Coumarin	π–σ (2)
	HDAC1	−9.0	His132	N=	H-bond
			Gly295	OH	H-bond
			Gly129	OH	H-bond
			Tyr297	N=	H-bond
			Tyr297	=O	H-bond
			Arg27	Coumarin	Cation-π (2)
			Leu265	Bromophenyl	π–σ
			Leu265	Thiazole	π-alkyl
			Phe198	CH_3	π–σ
			Phe198	Thiazole	π–π stack
			Phe141	CH_3	π–σ
			Phe141	Thiazole	π–π stack
			Met130	Phenyl	π-alkyl
			Leu23	Coumarin	π-alkyl
			Cys142	Coumarin	π-alkyl

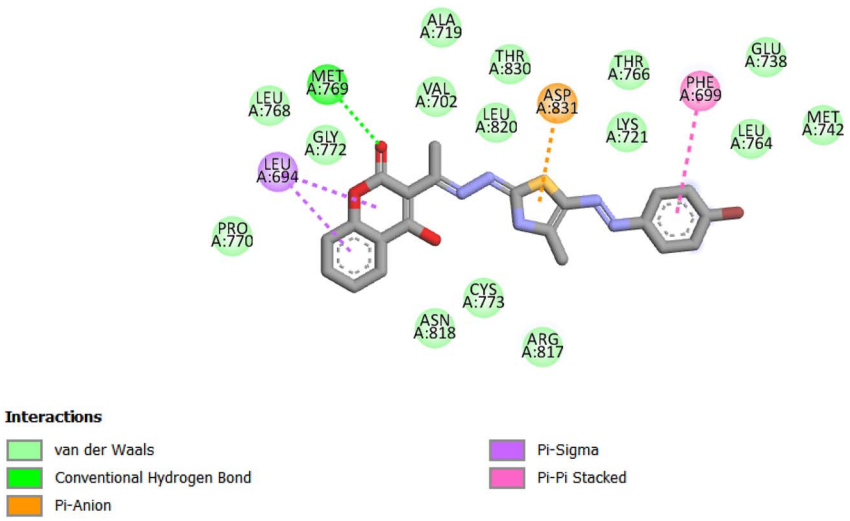

Fig. 7 2D interactions of compound **3m** within the EGFR active site.

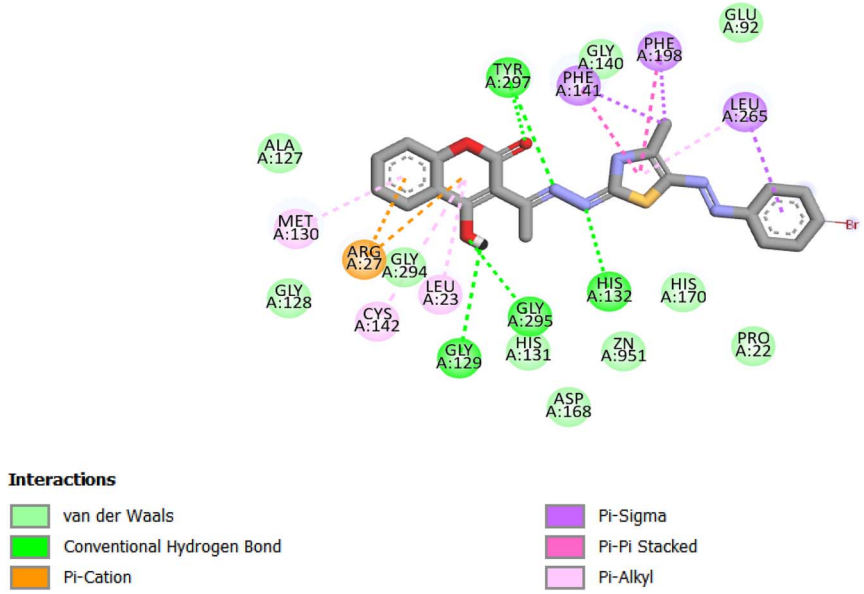

Fig. 8 2D interactions of compound **3m** within the HDAC active site.

3. Conclusion

In this study, dual EGFR/HDAC1 inhibitors were rationally designed as antitumor agents by relating the pharmacophoric features of both EGFR and HDAC1 inhibitors. This effort was prompted by researches that confirmed the overexpression of EGFR and HDAC1 isoforms in breast and colorectal cancers and the exceptional anticancer potential of dual EGFR/HDAC1 inhibitors in a variety of malignancies. As a result, a number of coumarin-based thiazole derivatives were synthesized to undergo a series of biological assays. Compounds **3m** and **3n** showed exceptional selectivity indices towards breast and colorectal cancers. In particular, further assays demonstrated the capacity of compound **3m** to selectively inhibit EGFR, HDAC1 and ERK and induce apoptosis and cell-cycle arrest at the G2/M phase, suggesting its remarkable cell-growth inhibitory effect. The *in vivo* study showed that compound **3m** was capable of inhibiting the cell growth by 60.61% in an Ehrlich ascites carcinoma cell model and decreasing the tumor size in an Ehrlich solid carcinoma cell model, verifying the *in vitro* results. Finally, docking of compound **3m** within the active sites of EGFR and HDAC revealed docking scores of −8.2 and −9.0 kcal mol^{-1}, respectively.

4. Materials and methods

4.1. Chemistry

All melting points were uncorrected and measured using an Electrothermal IA 9000 apparatus. The nuclear magnetic resonance spectra ^{1}HNMR (400 MHz) and ^{13}CNMR spectra (100 MHz) were recorded on a Bruker spectrometer using TMS as the internal standard. Mass spectrometry was carried out on the direct inlet part to mass analyzer in a Thermo Scientific GCMS model ISQ. The reactions were followed by TLC (silica gel, aluminum sheets 60 F254, Merck) using a toluene–ethylacetate mixture (8 : 2 v/v) as the eluent and sprayed with iodine-potassium iodide reagent. The purity of the newly synthesized compounds was assessed by TLC and elemental analysis and was found to be higher than 95%. Compounds **2a–c** were previously reported.[15]

4.1.1 Synthesis of 3-(-1-((5-(aryl)diazenyl)thiazol-2(3*H*)-ylidene)-hydrazono)ethyl)-4-hydroxy-coumarin derivatives (3a–o). A mixture of compounds **2a–c** (2.5 mmol) and appropriate hydrazonoyl chlorides (2.5 mmol) in dioxane (20 mL) containing triethylamine (0.25 mL, 1 mmol) was heated under reflux for 8–10 h and then cooled. The solution was poured onto crushed ice and concentrated hydrochloric acid. The produced solid was collected by filtration and crystallized from ethanol to give compounds **3a–o**.

4.1.2 4-Hydroxy-3-(-1-((-5-(-(4-methoxyphenyl)diazenyl)-4-methylthiazol-2(3*H*)-ylidene) hydrazono)ethyl)-2*H*-chromen-2-one (3a). Yield (89%); m.p. 95–7 °C. Anal. calcd for $C_{22}H_{19}N_5O_4S$ (449.48): C, 58.79; H, 4.26; N, 15.58; S, 7.13. Found: C, 58.88; H, 4.39; N, 15.66; S, 7.23. ^{1}H NMR (DMSO-d_6, δ, ppm): 2.68 (3H, s, CH_3), 2.72 (3H, s, CH_3), 3.84 (3H, s, OCH_3), 7.26–8.02 (10H, m, Ar–H, OH and NH). ^{13}C NMR (DMSO-d_6, δ, ppm): 12.12, 55.93, 91.17, 115.14, 116.87, 117.20, 119.17, 124.30, 125.25, 125.67, 133.73, 137.13, 145.10, 157.97, 161.08, 163.67.

4.1.3 4-Hydroxy-3-(-1-((-5-(-(4-methoxyphenyl)diazenyl)-3,4-dimethylthiazol-2(3*H*)-ylidene) hydrazono)ethyl)-2*H*-chromen-2-one (3b). Yield (88%); m.p. 219–20 °C. Anal. calcd for $C_{23}H_{21}N_5O_4S$ (463.51): C, 59.60; H, 4.57; N, 15.11; S, 6.92. Found: C, 59.69; H, 4.66; N, 15.20; S, 7.01. ^{1}H NMR (DMSO-d_6, δ, ppm): 2.68 (3H, s, CH_3), 2.72 (3H, s, CH_3), 3.57 (3H, s, CH_3), 3.84 (3H, s, OCH_3), 7.27–8.02 (9H, m, Ar–H and OH). ^{13}C NMR (DMSO-d_6, δ, ppm): 9.56, 16.48, 30.06, 56.03, 85.33, 114.70,

116.50, 117.29, 123.98, 125.28, 125.71, 133.82, 137.14, 152.55, 153.35, 154.71, 156.21, 160.46.

4.1.4 3-(1-((-3-Ethyl-5-(-(4-methoxyphenyl)diazenyl)-4-methylthiazol-2(3*H*)-ylidene) hydrazono)ethyl)-4-hydroxy-2*H*-chromen-2-one (3c). Yield (83%); m.p. 207–8 °C. Anal. calcd for $C_{24}H_{23}N_5O_4S$ (477.53): C, 60.36; H, 4.85; N, 14.67; S, 6.71. Found: C, 60.46; H, 4.92; N, 14.75; S, 6.80. ^{1}H NMR (DMSO-d_6, δ, ppm): 1.37–1.39 (3H, t, CH_3, $J = 7.16$ Hz), 2.68 (3H, s, CH_3), 2.72 (3H, s, CH_3), 3.85 (3H, s, OCH_3), 4.07–4.14 (2H, q, CH_2, $J = 7.16$ Hz), 7.27–8.02 (9H, m, Ar–H and OH). ^{13}C NMR (DMSO-d_6, δ, ppm): 9.56, 11.41, 12.64, 56.01, 87.91, 114.00, 115.51, 116.23, 125.00, 125.53, 127.23, 129.50, 131.49, 139.33, 144.28, 150.51, 153.92, 155.43, 157.32, 162.72.

4.1.5 3-(-1-((-5-(-(2,4-Dinitrophenyl)diazenyl)-4-methylthiazol-2(3*H*)-ylidene)hydrazono)ethyl)-4-hydroxy-2*H*-chromen-2-one (3d). Yield (89%); m.p. 113–4 °C. Anal. calcd for $C_{21}H_{15}N_7O_7S$ (509.45): C, 49.51; H, 2.97; N, 19.25; S, 6.29. Found: C, 49.59; H, 3.06; N, 19.35; S, 6.37. ^{1}H NMR (DMSO-d_6, δ, ppm): 2.69 (3H, s, CH_3), 2.73 (3H, s, CH_3), 7.34–8.96 (9H, m, Ar–H, OH and NH). ^{13}C NMR (DMSO-d_6, δ, ppm): 12.11, 16.45, 86.42, 116.99, 120.11, 123.81, 129.19, 129.77, 135.78, 137.29, 140.69, 144.77, 147.12, 150.08, 150.52, 158.15, 159.85, 164.64.

4.1.6 3-(-1-((-5-(-(2,4-Dinitrophenyl)diazenyl)-3,4-dimethylthiazol-2(3*H*)-ylidene)hydrazone) ethyl)-4-hydroxy-2*H*-chromen-2-one (3e). Yield (87%); m.p. 254–5 °C. Anal. calcd for $C_{22}H_{17}N_7O_7S$ (523.48): C, 50.48; H, 3.27; N, 18.73; S, 6.13. Found: C, 50.55; H, 3.36; N, 18.80; S, 6.21. ^{1}H NMR (DMSO-d_6, δ, ppm): 2.69 (3H, s, CH_3), 2.74 (3H, s, CH_3), 3.59 (3H, s, CH_3), 7.34–8.96 (8H, m, Ar–H and OH). ^{13}C NMR (DMSO-d_6, δ, ppm): 12.00, 13.39, 30.03, 76.53, 102.79, 106.53, 116.32, 118.46, 121.73, 124.86, 126.80, 128.87, 131.73, 132.29, 133.12, 138.01, 144.15, 150.01, 155.09, 157.21, 161.51, 164.46.

4.1.7 3-(-1-((-5-(-(2,4-Dinitrophenyl)diazenyl)-3-ethyl-4-methylthiazol-2(3*H*)-ylidene)hydrazono) ethyl)-4-hydroxy-2*H*-chromen-2-one (3f). Yield (88%); m.p. 143–5 °C. Anal. calcd for $C_{23}H_{19}N_7O_7S$ (537.50): C, 51.40; H, 3.56; N, 18.24; S, 5.96. Found: C, 51.48; H, 3.67; N, 18.30; S, 6.07. ^{1}H NMR (DMSO-d_6, δ, ppm): 1.17–1.21 (3H, t, CH_3, $J = 7.28$ Hz), 2.69 (3H, s, CH_3), 2.74 (3H, s, CH_3), 4.13–4.19 (2H, q, CH_2, $J = 7.12$ Hz), 7.34–8.96 (8H, m, Ar–H and OH). ^{13}C NMR (DMSO-d_6, δ, ppm): 11.23, 12.87, 14.34, 44.70, 80.03, 112.09, 112.94, 117.48, 120.10, 123.81, 125.71, 127.45, 129.76, 131.70, 135.78, 144.54, 146.24, 148.10, 150.09, 150.86, 158.82, 161.81, 164.41.

4.1.8 3-(-1-((-5-(-(4-Fluorophenyl)diazenyl)-4-methylthiazol-2(3*H*)-ylidene)hydrazono)ethyl)-4-hydroxy-2*H*-chromen-2-one (3g). Yield (85%); m.p. 133–5 °C. Anal. calcd for $C_{21}H_{16}FN_5O_3S$ (437.44): C, 57.66; H, 3.69; N, 16.01; S, 7.33. Found: C, 57.75; H, 3.77; N, 16.12; S, 7.41. ^{1}H NMR (DMSO-d_6, δ, ppm): 2.59 (3H, s, CH_3), 2.68 (3H, s, CH_3), 7.18–7.97 (10H, m, Ar–H, OH and NH). ^{13}C NMR (DMSO-d_6, δ, ppm): 12.12, 13.23, 78.48, 101.58, 115.04, 116.51, 116.70, 116.78, 123.41, 125.28, 125.65, 137.15, 139.22, 147.51, 154.40, 157.41, 159.79, 160.03, 163.92, 164.87.

4.1.9 3-(-1-((-5-(-(4-Fluorophenyl)diazenyl)-3,4-dimethylthiazol-2(3*H*)-ylidene)hydrazono)ethyl)-4-hydroxy-2*H*-chromen-2-one (3h). Yield (88%); m.p. 200–1 °C. Anal. calcd for $C_{22}H_{18}FN_5O_3S$ (451.47): C, 58.53; H, 4.02; N, 15.51; S, 7.10. Found: C, 58.61; H, 4.12; N, 15.59; S, 7.18. ^{1}H NMR (DMSO-d_6, δ, ppm): 2.76 (3H, s, CH_3), 2.86 (3H, s, CH_3), 3.56 (3H, s, CH_3), 7.19–7.95 (9H, m, Ar–H AND OH). ^{13}C NMR (DMSO-d_6, δ, ppm): 11.23, 15.70, 30.23, 78.91, 110.28, 110.97, 113.75, 117.81, 119.20, 121.80, 124.18, 128.08, 132.45,133.24, 144.12, 150.64, 156.13, 158.33, 159.09, 165.51, 168.79.

4.1.10 3-(-1-((-3-Ethyl-5-(-(4-fluorophenyl)diazenyl)-4-methylthiazol-2(3*H*)-ylidene)hydrazono) ethyl)-4-hydroxy-2*H*-chromen-2-one (3i). Yield (88%); m.p. 145–6 °C. Anal. calcd for $C_{23}H_{20}FN_5O_3S$ (465.12): C, 59.35; H, 4.33; N, 15.05; S, 6.89. Found: C, 59.44; H, 4.42; N, 15.16; S, 6.97. ^{1}H NMR (DMSO-d_6, δ, ppm): 1.38–1.41 (3H, t, CH_3, $J = 7.04$ Hz), 2.81 (3H, s, CH_3), 2.86 (3H, s, CH_3), 4.14–4.20 (2H, q, CH_2, $J = 7.40$ Hz), 7.19–7.92 (9H, m, Ar–H and OH). ^{13}C NMR (DMSO-d_6, δ, ppm): 11.63, 14.23, 18.51, 44.53, 73.97, 103.42, 113.40,116.36, 116.59, 116.77, 123.69, 125.70, 129.51, 134.69, 136.44, 142.62, 150.21, 156.82, 157.48, 160.78, 162.81, 169.26.

4.1.11 3-(-1-((-5-(-(4-Chlorophenyl)diazenyl)-4-methylthiazol-2(3*H*)-ylidene)hydrazono)ethyl)-4-hydroxy-2*H*-chromen-2-one (3j). Yield (86%); m.p. 152–3 °C. Anal. calcd for $C_{21}H_{16}ClN_5O_3S$ (453.90): C, 55.57; H, 3.55; N, 15.43; S, 7.06. Found: C, 55.67; H, 3.63; N, 15.50; S, 7.12. ^{1}H NMR (DMSO-d_6, δ, ppm): 2.60 (3H, s, CH_3), 2.69 (3H, s, CH_3), 7.18–7.97 (10H, m, Ar–H, OH and NH). ^{13}C NMR (DMSO-d_6, δ, ppm): 12.44, 13.91, 78.36, 101.44, 117.31, 123.91, 124.44, 124.78, 125.70, 127.63, 129.64, 132.39, 137.12, 142.27, 154.83, 157.41, 159.75, 163.94, 164.87.

4.1.12 3-(-1-((-5-(-(4-Chlorophenyl)diazenyl)-3,4-dimethylthiazol-2(3*H*)-ylidene)hydrazono)ethyl)-4-hydroxy-2*H*-chromen-2-one (3k). Yield (90%); m.p. 122–3 °C. Anal. calcd for $C_{22}H_{18}ClN_5O_3S$ (467.93): C, 56.47; H, 3.88; N, 14.97; S, 6.85. Found: C, 56.55; H, 3.94; N, 15.06; S, 6.93. ^{1}H NMR (DMSO-d_6, δ, ppm): 2.78 (3H, s, CH_3), 2.86 (3H, s, CH_3), 3.58 (3H, s, CH_3), 7.19–7.95 (9H, m, Ar–H and OH). ^{13}C NMR (DMSO-d_6, δ, ppm): 17.44, 18.06, 30.06, 79.11, 101.93, 117.63, 123.78, 125.25, 125.69, 129.00, 129.61, 137.15, 141.98, 154.65, 159.86, 160.93, 163.07, 165.26.

4.1.13 3-(-1-((-5-(-(4-Chlorophenyl)diazenyl)-3-ethyl-4-methylthiazol-2(3*H*)-ylidene)hydrazono) ethyl)-4-hydroxy-2*H*-chromen-2-one (3l). Yield (88%); m.p. 199–200 °C. Anal. calcd for $C_{23}H_{20}ClN_5O_3S$ (481.95): C, 57.32; H, 4.18; N, 14.53; S, 6.65. Found: C, 57.41; H, 4.23; N, 14.60; S, 6.73. ^{1}H NMR (DMSO-d_6, δ, ppm): 1.37–1.40 (3H, t, CH_3, $J = 7.2$ Hz), 2.81 (3H, s, CH_3), 2.84 (3H, s, CH_3), 4.13–4.19 (2H, q, CH_2, $J = 7.40$ Hz), 7.19–7.93 (9H, m, Ar–H and OH). ^{13}C NMR (DMSO-d_6, δ, ppm): 12.23, 13.88, 17.71, 41.41, 78.02, 101.96, 117.34, 123.97, 125.27, 126.87, 128.85, 129.63, 130.66, 137.17, 141.99, 152.83, 154.48, 154.67, 159.71, 165.27.

4.1.14 3-(-1-((-5-(-(4-Bromophenyl)diazenyl)-4-methylthiazol-2(3*H*)-ylidene)hydrazono)ethyl)-4-hydroxy-2*H*-chromen-2-one (3m). Yield (90%); m.p. 124–5 °C. Anal. calcd for $C_{21}H_{16}BrN_5O_3S$ (498.35): C, 50.61; H, 3.24; N, 14.05; S, 6.43. Found: C, 50.69; H, 3.31; N, 14.11; S, 6.52. ^{1}H NMR (DMSO-d_6, δ, ppm): 2.60 (3H, s, CH_3), 2.70 (3H, s, CH_3), 7.17–7.95 (10H, m, Ar–H, OH and NH). ^{13}C NMR (DMSO-d_6, δ, ppm): 11.23, 13.45, 73.56, 96.66, 117.30, 124.08, 125.32, 127.73, 128.41, 129.82, 132.51, 132.68, 142.39, 152.05, 152.81, 153.65, 158.45, 161.95, 166.43. MS m/z (R.A. %): 497, 499 (M^+, M^++2) (22.14, 18.82%).

4.1.15 3-(-1-((-5-(-(4-Bromophenyl)diazenyl)-3,4-dimethylthiazol-2(3*H*)-ylidene)hydrazono)ethyl)-4-hydroxy-2*H*-chromen-2-one (3n). Yield (90%); m.p. 102–3 °C. Anal. calcd for $C_{22}H_{18}BrN_5O_3S$ (512.38): C, 51.57; H, 3.54; N, 13.67; S, 6.26. Found: C, 51.66; H, 3.62; N, 13.74; S, 6.35. ^{1}H NMR (DMSO-d_6, δ, ppm): 2.75 (3H, s, CH_3), 2.84 (3H, s, CH_3), 3.57 (3H, s, CH_3), 7.17–7.94 (9H, m, Ar–H and OH). ^{13}C NMR (DMSO-d_6, δ, ppm): 13.11, 17.48, 30.09, 78.98, 101.89, 117.34, 122.88, 124.07, 125.27, 125.72, 132.75,137.17, 149.67, 151.16, 153.36, 158.28, 161.04, 162.34, 167.87. MS *m*/*z* (R.A. %): 511, 513 (M^+, M^++2) (27.88, 30.36%).

4.1.16 3-(-1-((-5-(-(4-Bromophenyl)diazenyl)-3-ethyl-4-methylthiazol-2(3*H*)-ylidene)hydrazono) ethyl)-4-hydroxy-2*H*-chromen-2-one (3o). Yield (90%); m.p. 149–50 °C. Anal. calcd for $C_{23}H_{20}BrN_5O_3S$ (526.41): C, 52.48; H, 3.83; N, 13.30; S, 6.09. Found: C, 52.55; H, 3.92; N, 13.38; S, 6.16. ^{1}H NMR (DMSO-d_6, δ, ppm): 1.37–1.40 (3H, t, CH_3, $J = 7.16$ Hz), 2.82 (3H, s, CH_3), 2.85 (3H, s, CH_3), 4.17–4.23 (2H, q, CH_2, $J = 7.64$ Hz), 7.16–7.96 (9H, m, Ar–H and OH). ^{13}C NMR (DMSO-d_6, δ, ppm): 12.07, 14.04, 16.23, 42.72, 78.71, 100.07, 117.31, 124.10, 125.25, 125.74, 128.41, 129.82, 132.51, 142.41, 150.95, 154.78, 158.01, 159.24, 162.25, 165.66.

4.2. Biology

4.2.1 *In vitro* studies

4.2.1.1. Antiproliferative activity. Roswell Park Memorial Institute (RPMI) 1640 medium was purchased from Sigma Chem. Co. (St. Louis, MO, USA). Fetal bovine serum (FBS) and fetal calf serum (FCS) were purchased from Gibco, UK. Dimethyl sulfoxide (DMSO) and methanol were of HPLC grade, and all other reagents and chemicals were of analytical reagent grade. MCF-7 (human breast adenocarcinoma), HCT116 (human colorectal carcinoma) and the normal human skin fibroblast (BJ-1) cell lines were purchased from the American Type Culture Collection (Rockville, MD, USA) and maintained in the RPMI-1640 medium, which was supplemented with 10% heat-inactivated FBS, 100 U per mL penicillin, and 100 U per mL streptomycin. The cells were grown at 37 °C in a humidified atmosphere of 5% CO_2. All experiments were conducted thrice in triplicate ($n = 3$). All the values were represented as means ± SD.

To determine the effect of each synthesized compound on membrane permeability in MCF-7 and HCT-116 cancer cell lines and BJ-1 normal cell line, a lactate dehydrogenase (LDH) release assay was conducted.[31–35] The cells were seeded in 24-well culture plates at a density of 1×10^4 cells per well with a volume of 500 μL and allowed to grow for 18 h before treatment. After treatment with different concentrations of each compound or doxorubicin® (positive control), the plates were incubated for 48 h. Then, the supernatant (40 μL) was transferred to a new 96-well plate to determine the LDH release, and 6% Triton X-100 (40 μL) was added to the original plate to determine the total LDH. An aliquot of 0.1 M potassium phosphate buffer (100 μL, pH 7.5) containing 4.6 mM pyruvic acid was mixed with the supernatant using repeated pipetting. Then, 0.1 M potassium phosphate buffer (100 μL, pH 7.5) containing 0.4 mg mL^{-1} of reduced β-NADH was added to the wells. The kinetic changes were read for 1 min using the ELISA microplate reader under absorbance at a wavelength of 340 nm. This procedure was repeated with 40 μL of the total cell lysate to determine the total LDH. The percentage of LDH released was determined by dividing the LDH released into the media by the total LDH following cell lysis in the same well.

4.2.1.2. EGFR inhibition assay. The kinase activity assay of the epidermal growth factor receptor (EGFR) was performed according to the manufacturer's instructions using the EGFR kinase assay kit (BPS Bioscience, CA # 40321). The kit uses Kinase-Glo™ MAX as the detection reagent (Promega #V6071). Results of the tested compound were assessed by measuring the luminescence using a ROBONIK P2000 ELIZA reader at 450 nm.

4.2.1.3. HDAC1 inhibition assay. The histone deacetylase 1 (HDAC1) assay was conducted according to the manufacturer's instructions using a fluorogenic HDAC1 Assay Kit (BPS Bioscience, CA # 50061). The examined compound's activity was determined by measuring the fluorescence using a Bio-Tek fluorescent microplate reader.

4.2.1.4. In vitro ERK activity assay. An ERK1 Kinase Assay Kit was used to measure the ERK1 (extracellular signal-regulated kinase 1) inhibition according to the manufacturer's instructions (Chemi-Verse, CA # 82282), using ADP-Glo™ as the detection reagent.

4.2.1.5. Cell-cycle inhibition and apoptosis assay. MCF-7 cells were seeded at 8×10^4 cells per well in a six well plate and incubated overnight at 37 °C. The cells were then treated with compound **3m** and incubated for 48 h for treatment. At the end of the incubation time, the cell pellets were collected and centrifuged at 300 × *g* for 5 min. For cell-cycle analysis, the cell pellets were fixed in 70% ethanol on ice for 15 min. The collected pellets were incubated with propidium iodide (PI) staining solution (50 μg mL^{-1} PI, 0.1 mg mL^{-1} RNaseA, and 0.05% Triton X-100) at room temperature for 1 h. Apoptosis detection was performed using FITC Annexin-V/PI kit (Becton Dickinson, Franklin Lakes, NJ, USA) following a previous protocol. The sample was analyzed by flow cytometry on a Beckman Coulter Gallios (Beckman Coulter, Brea, CA, USA) within 1 h of staining, and the data were analyzed using Kaluza v1.2 (Beckman Coulter).[36]

4.2.2 *In vivo* studies

4.2.2.1. Animals. Male and female Balb-c mice, 8–10 weeks of age, were purchased from the laboratory animal unit at the National Research Centre, Egypt. The mice were housed under standardized conditions at 26 ± 2 °C, with a normal 12-h light/dark cycle and free access to food and water. The animal experiment was performed according to the ARRIVE guidelines for the proper conduct of animal experiments, following the approval of the Ethical Committee of the National Research Centre (Ethical Code#13010137-4).

4.2.2.2. Maintenance and inoculation of Ehrlich tumor cells. The Ehrlich ascites tumor, originating from a spontaneous murine mammary adenocarcinoma, was maintained in its ascitic form in healthy female Balb-c mice *via* successive intraperitoneal (i.p.) passages, as previously described.[37] EAC cells were then collected from the peritoneal cavity following the

serial passages, rinsed with phosphate-buffered saline (PBS), and centrifuged at 1200×*g* for 10 minutes. Cell viability was assessed using the trypan blue exclusion assay, ensuring over 95% viability for subsequent experiments.

4.2.2.3. Ehrlich ascites carcinoma (EAC) model. Female Balb-c mice (25 ± 3 g body weight) were inoculated with viable EAC cells (1×10^6 cells) in 100 μL of PBS by intraperitoneal (i.p.) injection into the peritoneal cavity to induce ascites.

Three days following EAC inoculation, all the mice were divided into five groups ($n = 8$ per group), as detailed previously, and then treated intraperitoneally with DMSO (vehicle), doxorubicin, compound **3m**, or compound **3n**. At the end of the designated treatment protocol for each group, ascitic fluid was collected from the peritoneal cavity using a sterile syringe. The ascitic fluid was centrifuged at 1200×*g* for 10 min, and subsequently, supernatants were separated and cells were washed with PBS.

• Cell viability assay: total viable EAC cells in the ascitic fluid were counted using the trypan blue exclusion assay. A sample of the ascitic fluid was mixed with an equal volume of 0.4% trypan blue solution and counted under a light microscope using a hemocytometer. Viable cells (unstained) and non-viable cells (stained) were counted for each sample.

• Growth inhibition: cell-growth inhibition was calculated by comparing the viable cell counts between the treated groups and the EAC control group using the following formula:

Growth inhibition (%) = [(viable cell count in EAC control group − viable cell counts in treated group)/viable cell count in EAC control group] × 100.

4.2.2.4. Ehrlich solid carcinoma (ESC) model. Male Balb/c mice (25–28 g body weight) were used for this part of the study. For the induction of solid carcinoma, EAC cells harvested from the peritoneal cavity of donor mice previously inoculated with EAC were washed with phosphate-buffered saline (PBS) and counted using a trypan blue exclusion assay. Only suspensions with greater than 95% cell viability were used. The cells were then resuspended in PBS and injected intramuscularly into the thigh of each mouse to induce solid tumor formation (2×10^6 cells in 0.2 mL of PBS). Drug treatment began five days post inoculation to allow for initial tumor establishment. The mice were treated intratumorally with DMSO (vehicle), doxorubicin, compound **3m**, or compound **3n**. At the end of the designated treatment protocol for each group, the mice were sacrificed and the tumor masses were collected.

Tumor Volume Assessment: the tumor size was measured using a digital caliper. Both the width and length diameters of the tumor were recorded. The width is considered the smallest diameter of the tumor, and the length is the largest diameter of the tumor.

Tumor volume was estimated using the standard formula for solid tumors:

$$\text{Tumor volume (mm}^3) = \tfrac{1}{2} \times (\text{width})^2 \times (\text{length})$$

4.2.3 Statistical analysis. All *in vitro* experiments were conducted in triplicate ($n = 3$). All the values were represented as mean ± SD. Significant differences between the means of parameters and the IC_{50} values were determined by probit analysis using the SPSS software program (SPSS Inc., Chicago, IL).

4.3. Molecular docking

Autodock Vina software was used to perform the docking study with a grid box of 25^3 Å^3 centered on a co-crystalized ligand in the active site of EGFR and histone deacetylase homologue, which were retrieved from the protein data bank (PDB ID: 1M17)[38] and (PDB ID: 1C3S),[39] respectively, using an exhaustiveness value of 16. The compound was created using Marvin sketch. Autodock tools were utilized to create the required pdbqt files since Vina Autodock requires the receptor and ligands to be in pdbqt format. The selected compound was docked into the predetermined active site for the targeted proteins. The screening of the molecule was completed using PyRx 0.8. Validation was achieved by redocking of the co-crystalized ligand and calculating the RMSD using the DockRMSD server. Finally, the free Biovia Discovery Studio 2021 visualizer was used to demonstrate the docking poses.

Conflicts of interest

The authors have declared that there are no actual or potential conflicts of interest and have approved the article.

Data availability

The data supporting this article, including ^{1}HMNR and ^{13}CMNR spectra of all the newly synthesized compounds, have been included as part of the SI. See DOI: **https://doi.org/10.1039/d5ra04395f**.

Acknowledgements

This research article was funded by the NRC, Cairo, Egypt (2022–2024), through project no. 13010137 entitled "Synthesis and computational studies of new naturally derived anticancer heterocyclic compounds".

References

1 V. T. DeVita and E. Chu, *Cancer Res.*, 2008, **68**, 8643.
2 A. Mitra, L. Mishra and S. Li, *Oncotarget*, 2015, **6**, 10697.
3 P. Blume-Jensen and T. Hunter, *Nature*, 2001, **411**, 355.
4 R. E. Favoni and A. de Cupis, *Pharmacol. Rev.*, 2000, **52**, 179.
5 D. Hanahan and R. A. Weinberg, *Cell*, 2011, **144**, 646.
6 R. Z. Batran, S. M. El-Daly, W. A. El-Kashak and E. Y. Ahmed, *Chem. Biol. Drug Des.*, 2022, **99**, 470.
7 N. Garmpis, C. Damaskos, D. Dimitroulis, G. Kouraklis, A. Garmpi, P. Sarantis, E. Koustas, A. Patsouras, I. Psilopatis, E. A. Antoniou, M. V Karamouzis, K. Kontzoglou and A. Nonni, *J. Pers. Med.*, 2022, **12**, 1672.
8 P. Wang, Z. Wang and J. Liu, *Mol. Cancer*, 2020, **19**, 5.
9 Y. Chen, S. Zhang, Z. Li, B. Yin, Y. Liu and L. Zhang, *ChemMedChem*, 2023, **18**, e202300281.

10 C.-W. Chou, M.-S. Wu, W.-C. Huang and C.-C. Chen, *PLoS One*, 2011, **6**, e18087.
11 W. Yu, W. Lu, G. Chen, F. Cheng, H. Su, Y. Chen, M. Liu and X. Pang, *Br. J. Pharmacol.*, 2017, **174**, 3608.
12 A. A. Nasser, I. H. Eissa, M. R. Oun, M. A. El-Zahabi, M. S. Taghour, A. Belal, A. M. Saleh, A. B. M. Mehany, H. Luesch, A. E. Mostafa, W. M. Afifi, J. R. Rocca and H. A. Mahdy, *Org. Biomol. Chem.*, 2020, **18**, 7608.
13 S. A. Elmetwally, K. F. Saied, I. H. Eissa and E. B. Elkaeed, *Bioorg. Chem.*, 2019, **88**, 102944.
14 C. Ma, M. S. Taghour, A. Belal, A. B. M. Mehany, N. Mostafa, A. Nabeeh, I. H. Eissa and A. A. Al-Karmalawy, *Front. Chem.*, 2021, **9**, 725135.
15 A. Carneiro, M. J. Matos, E. Uriarte and L. Santana, *Molecules*, 2021, **26**, 501.
16 E. M. Eliwa, M. Frese, A. H. Halawa, M. M. Soltan, L. V Ponomareva, J. S. Thorson, K. A. Shaaban, M. Shaaban, A. M. El-Agrody and N. Sewald, *Green Chem. Lett. Rev.*, 2021, **14**, 578.
17 R. Pili, O. Al-Ustwani, N. Gupta and L. Shen, *Onco. Targets. Ther.*, 2014, **7**, 223.
18 C. Seidel, M. Schnekenburger, C. Zwergel, F. Gaascht, A. Mai, M. Dicato, G. Kirsch, S. Valente and M. Diederich, *Bioorg. Med. Chem. Lett.*, 2014, **24**, 3797.
19 D. T. Anh, P.-T. Hai, L.-T.-T. Huong, E. J. Park, H. W. Jun, J. S. Kang, J.-H. Kwon, D. T. M. Dung, V. T. Anh, V. T. M. Hue, S.-B. Han and N.-H. Nam, *Bioorg. Chem.*, 2020, **101**, 103988.
20 T. Tung, D. Kim Oanh, P. Phuong Dung, V. My Hue, S. Park, B. Han, Y. Kim, J.-T. Hong, S.-B. Han and N.-H. Nam, *Med. Chem.*, 2013, **9**, 1051.
21 X. Cao and Y. Gong, *Future Med. Chem.*, 2024, **16**, 469.
22 G. Costanzo, R. Buccheri, G. Cosentino, C. Reale, S. Zuccalà, A. Marrazzo, E. Amata, A. Rescifina and L. Pasquinucci, *Eur. J. Med. Chem.*, 2025, **298**, 117998.
23 V. Pardo-Jiménez, P. Navarrete-Encina and G. Díaz-Araya, *Molecules*, 2019, **24**, 4040739.
24 R. Z. Batran, E. Y. Ahmed, H. M. Awad, K. A. Ali and N. A. Abdel Latif, *RSC Adv.*, 2023, **13**, 29070.
25 M. T. Gabr, N. S. El-Gohary, E. R. El-Bendary, M. M. El-Kerdawy and N. Ni, *Excli J.*, 2017, **16**, 1114.
26 R. S. Iyer, S. R. Needham, I. Galdadas, B. M. Davis, S. K. Roberts, R. C. H. Man, L. C. Zanetti-Domingues, D. T. Clarke, G. O. Fruhwirth, P. J. Parker, D. J. Rolfe, F. L. Gervasio and M. L. Martin-Fernandez, *Nat. Commun.*, 2024, **15**, 2130.
27 Y. Wu, J. Xu, Y. Liu, Y. Zeng and G. Wu, *Front. Oncol.*, 2020, **10**, 592853.
28 R. Z. Batran, E. Y. Ahmed, E. S. Nossier, H. M. Awad and N. A. Abdel Latif, *J. Mol. Struct.*, 2024, **1305**, 137790.
29 R. Z. Batran, M. M. Elghonemy, E. Y. Ahmed, S. M. El-Daly, H. M. Awad and N. A. Abdel Latif, *J. Mol. Struct.*, 2024, **1318**, 139123.
30 R. Z. Batran, E. Y. Ahmed, H. M. Awad and N. A. Abdel Latif, *RSC Adv.*, 2024, **14**, 22434.
31 S. F. Mohamed, E. R. Kotb, E. A. Abd El-Meguid and H. M. Awad, *Res. Chem. Intermed.*, 2017, **43**, 437.
32 M. E. Haiba, E. S. Al-Abdullah, N. S. Ahmed, H. A. Ghabbour and H. M. Awad, *J. Mol. Struct.*, 2019, **1195**, 702.
33 M. A. A. Radwan, F. M. Alminderej and H. M. Awad, *Molecules*, 2020, **25**, 255.
34 A. A. S. Ahmed, H. M. Awad, I. E.-T. El-Sayed and A. A. El Gokha, *J. Iran. Chem. Soc.*, 2020, **17**, 1211.
35 D. H. Elnaggar, N. A. Abdel Hafez, H. R. M. Rashdan, N. A. M. Abdelwahed, H. M. Awad and K. A. Ali, *Mini-Reviews Med. Chem.*, 2019, **19**, 1717.
36 S. M. El-Daly, M. T. Abo-Elfadl, J. Hussein and M. A. M. Abo-Zeid, *Life Sci.*, 2023, **315**, 121320.
37 A. Z. Salem, D. Medhat, S. A. Fathy, M. R. Mohamed, Z. El-Khayat and S. M. El-Daly, *Mol. Biol. Rep.*, 2021, **48**, 6845.
38 J. Stamos, M. X. Sliwkowski and C. Eigenbrot, *J. Biol. Chem.*, 2002, **277**, 46265.
39 M. S. Finnin, J. R. Donigian, A. Cohen, V. M. Richon, R. A. Rifkind, P. A. Marks, R. Breslow and N. P. Pavletich, *Nature*, 1999, **401**, 188.